electronics

Article

# High-Capacity Double-Sided Square-Mesh-Type Chipless RFID Tags

**Muhammad Noman [1], Usman A. Haider [1], Hidayat Ullah [1], Muhammad Ikram [2], Hatem Rmili [3,4] and Farooq A. Tahir [1,*]**

1 School of Electrical Engineering and Computer Science, National University of Sciences and Technology, Islamabad 44000, Pakistan
2 School of Information Technology and Electrical Engineering, University of Queensland (UQ), Brisbane, QLD 4072, Australia
3 K.A. CARE Energy Research and Innovation Center, King Abdulaziz University, Jeddah 21589, Saudi Arabia
4 Electrical and Computer Engineering Department, Faculty of Engineering, King Abdulaziz University, Jeddah 21589, Saudi Arabia
* Correspondence: farooq.tahir@seecs.edu.pk; Tel.: +92-333-669-2822

**Abstract:** This paper presents a novel methodology for designing high-capacity frequency domain chipless RFID tags based on the backscattering principle. The tag consists of multiple square open-loop resonators loaded with a varying number of square metallic patches to form a mesh structure. Thus, in contrast to conventional designs, the overall physical size of each resonator remains fixed and does not change with respect to its operating resonant frequency. The RCS response of the proposed tag can be easily manipulated by varying the loading factor of each resonator. The tag size is further miniaturized by placing resonators on both sides of the substrate used. The tag configuration with resonators arranged in the form of a single row ($4 \times 1$) printed on both sides of the substrate is finally chosen for maximum robustness and efficiency. The frequency shift coding (FSC) technique is used to encode more than one bit per resonator by using segments within sub-bands. The proposed tag encodes 16-bit data in a frequency band from 5.9 to 10.5 GHz and has a very high code density of 23.51 bits/cm$^2$ and a spectral efficiency of 3.47 bits/GHz. The design methodology is novel and leads to a very efficient chipless RFID tag that can be used in a variety of high-data-capacity applications.

**Keywords:** tag; backscattering; chipless radio frequency identification; RFID; RCS; frequency shift coding; miniaturization



**Citation:** Noman, M.; Haider, U.A.; Ullah, H.; Ikram, M.; Rmili, H.; Tahir, F.A. High-Capacity Double-Sided Square-Mesh-Type Chipless RFID Tags. *Electronics* **2023**, *12*, 1371. https://doi.org/10.3390/electronics12061371

Academic Editor: Christos J. Bouras

Received: 20 November 2022
Revised: 7 February 2023
Accepted: 24 February 2023
Published: 13 March 2023



## 1. Introduction

Chipless tags for radio frequency identification (RFID) have emerged as a very hot topic of research within the scientific community in recent years. Any RFID system mainly consists of three components: the tag, the reader and a computer. The chipless radio frequency identification (CRFID) system does not have any silicon integrated circuit (IC) chip for data storage. Electromagnetic signatures from the tag are used to decode the encoded information [1]. Many advantages make this technology superior to the conventional chip-based RFID system, such as its low-cost, reduced tag size, lack of line-of-sight requirements, longer life span and direct printability [2,3]. CRFID tags are divided into two main categories based on the design methods: (1) semi-passive and (2) fully-passive. Due to the absence of an IC chip, data encoding is very challenging in these types of tags. For this purpose, different coding techniques have been proposed in the literature. Time domain (TD) and frequency domain (FD) encoding schemes are of particular focus.

In the recent literature, many chipless tags based on frequency and time domain techniques have been proposed. Tags in which a multi resonator structure is used to encode the data have been presented [4–7]. In these types of tags, information is encoded using the FD technique, where the presence and absence of the resonant peaks are encoded as '1' and '0', respectively. In another method presented in [8], open stub resonators are used to design chipless tags. In [9,10], the TD technique was used to encode the data by using the reflected signal from discontinuities placed at specified locations in the structure. These tags have a high data capacity, but their large size and high cost make them unsuitable for many applications.

CRFID tags based on the FD technique can be divided into two types: (1) retransmission-based and (2) backscattered-based. Retransmission-based tags consist of three major parts: the transmitting antenna (Tx), the receiving antenna (Rx), and a multi-resonator circuit. The Rx receives an incident signal from a reader, and Tx retransmits the tag's encoded information extracted from the multi-resonating structure. These tags have excellent encoding capabilities and a longer read range than other multi-resonator-based tags, but they have a large size and are expensive [11,12]. In contrast, backscattering tags do not need an antenna to transmit and receive EM signals, so the overall size of the tag is reduced. Each resonator acts as a transmitting and receiving antenna as well. Usually, each resonator obtains an incident signal from a reader and reflects the signal with encoded information. The response of these tags is measured as radar cross section (RCS). These tags are cost-effective and are easy to design and manufacture [13,14].

Various methodologies have been proposed to design backscattering (or RCS-based) chipless tags. This has been followed by different encoding techniques to enhance the overall storage capacity of the tags [15,16]. In [17], C-shaped resonators were used to design backscattering chipless tags. These tags have a low code density of 2.86 bits/cm$^2$ and a high spectral efficiency of 4.58 bits/GHz. A tag with a very low code density of 1.25 bits/cm$^2$ and a high spectral efficiency of 5 bits/GHz was proposed in [18]. In another tag [19], an impedance-loaded circular ring resonator with a very low code density of 2.63 bits/cm$^2$ was proposed. Moreover, tags with dual-polarized features have been recently presented. These tags include L-shaped resonators [20] with a code density of 9.45 bits/cm$^2$ and nested square loop resonators [21] with a code density of 12 bits/cm$^2$. A miniaturized open-loop resonator with a tag size of 6.6 $\times$ 10.8 mm$^2$ with a high code density of 4.99 bits/cm$^2$ using a very complex optimization technique was discussed in [22]. Several tags have a high spectral efficiency but a very low code density due to their large size [23–27]. This drawback limits the widespread usage of these tags where the tagged item encapsulates a small area. Some recently reported chipless RFID tag designs are L-shaped slot resonators [28], trefoil-shaped slot resonators [29], comb-shaped tags [30] and half octagonal ring resonators [31].

This paper presents a frequency domain RCS-based chipless tag using a novel design methodology. The tag is composed of square open-loop resonators with a size of 3.8 $\times$ 3.8 mm$^2$. The open-loop resonator is sequentially loaded with small square metallic patches to systematically produce resonances at different frequencies. This topology is simple and very effective, which leads to a square mesh of microstrip resonators. This technique provides great design flexibility while keeping the physical size of the resonator fixed. These sequentially loaded square mesh resonators are then placed on the front and backside of the substrate for maximum space utilization and minimum tag size. To further enhance the coding capacity of the proposed tag, frequency shift coding (FSC) is used. The proposed tag achieves a very high code density of 23.51 bits/cm$^2$ and a spectral efficiency of 3.47 bits/GHz in comparison with many recently published chipless tags in the 5.9–10.5 GHz frequency range.

## 2. Tag Design

The proposed tag is modeled on Rogers RT6035HTC substrate with a thickness t = 0.762 mm, permittivity $\varepsilon_r$ = 3.5 and loss tangent tan$\delta$ = 0.0013. Generally, in designing FD-based chipless tags, a shift in the resonance frequency is achieved by changing the size of the resonator. In this paper, a new approach is proposed that does not require any change in the size of the resonator for a shift in resonance frequency. This shift in resonance frequency is achieved by loading a square open-loop resonator with small square metallic patches. The patches are placed in a grid of small cells in an alternating way, resulting in a mesh structure.

The step-by-step design methodology of the proposed tag is shown in Figure 1. Initially, a square open-loop resonator is designed to resonate at the desired lowest frequency, as shown in Figure 1a. In the second stage, an empty area inside the square open-loop resonator is equally distributed into small unit cells with a size of $0.22 \times 0.22$ mm$^2$. The grid is shown in Figure 1b. Finally, multiple empty unit cells are sequentially but alternately filled with metal, as shown in Figure 1c. Consequently, a fully loaded square mesh open-loop resonator is formed. The optimized parameters of the final design are l = 3.33 mm, w = 0.25 mm and L = W = 3.8 mm. The backside of the resonator is kept void of the metal.

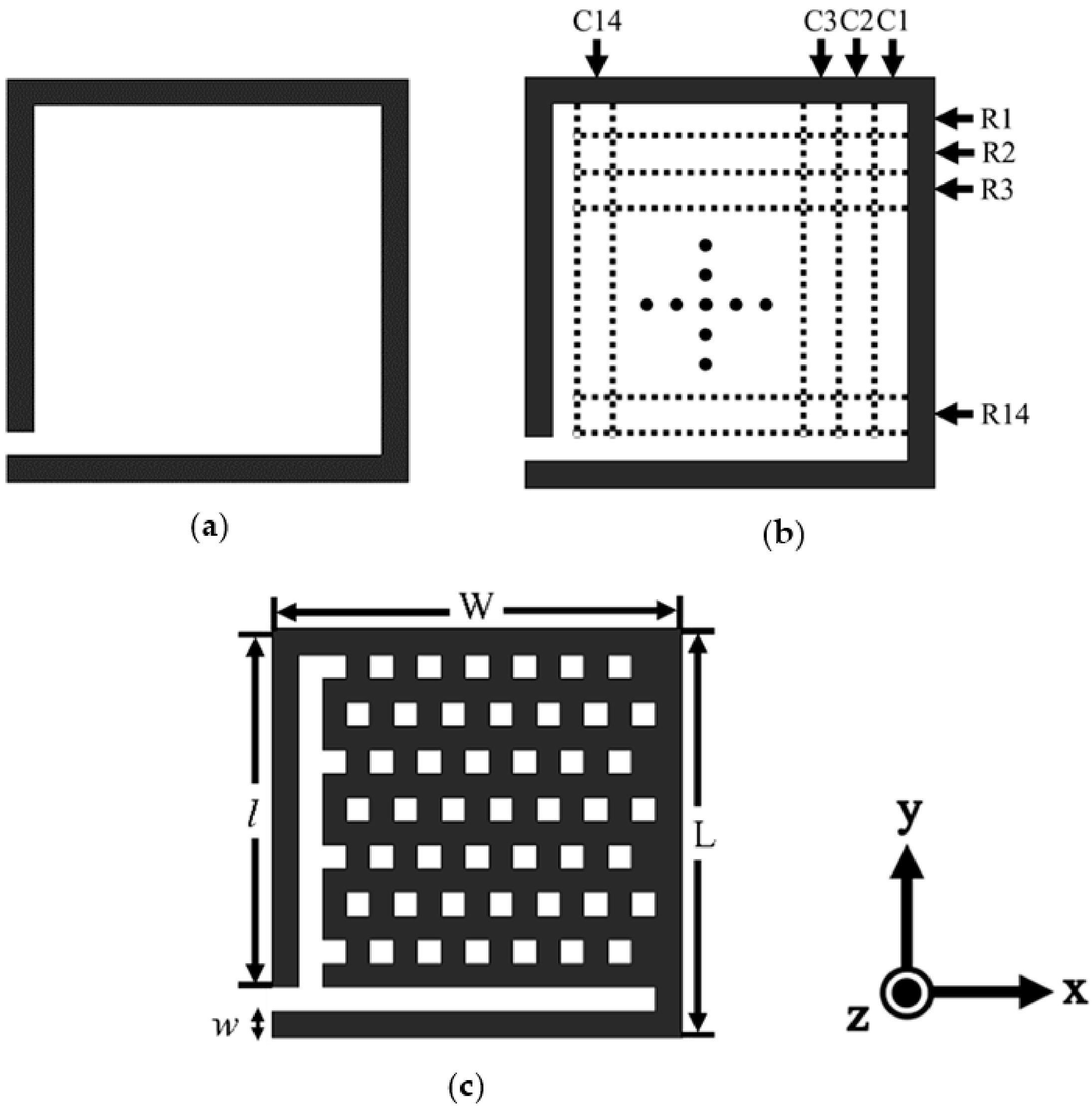


**Figure 1.** Metallic loading in square open-loop resonator: (**a**) square open-loop resonator; (**b**) equally divided small cell grid; (**c**) geometry of square mesh open-loop resonator.

The working mechanism of the proposed tag is analyzed in different steps. First, the performance of the empty square open-loop resonator of Figure 1a is analyzed. The RCS response of this basic open-loop resonator is plotted versus frequency by changing the value of a small gap "g", as shown in Figure 2. It can be observed that, as the value of "g" increases, the RCS response shifts towards a higher frequency. Hence, any value of the gap can be selected to operate the tag at any desired frequency. Here, the value of g = 0.22 mm is chosen.

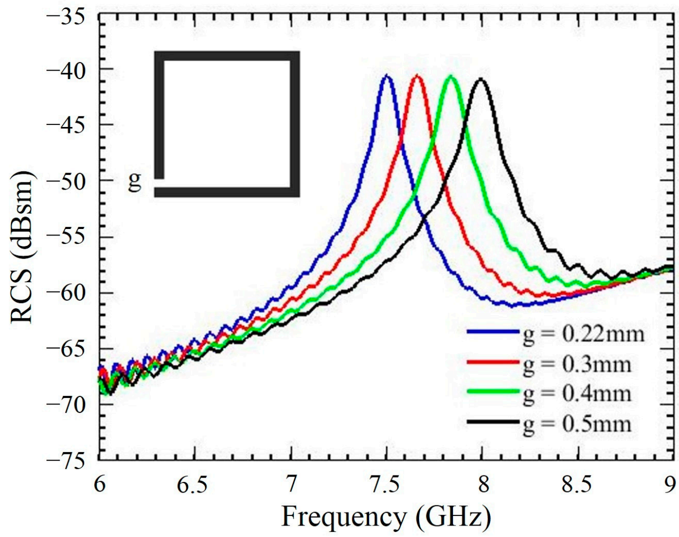


**Figure 2.** Geometry and simulated RCS response of open-loop resonator.

The empty area inside the square open-loop resonator is then equally divided into a grid of 196 small unit cells. The grid consists of 14 columns and 14 rows, labeled C1–C14 and R1–R14, respectively, as shown in Figure 1b. Finally, to obtain a shifted resonance response, a specific metal loading approach is used. Starting from the top right cell and moving toward the left side, multiple unit cells of R1 are filled with metal. This is referred to as a loading of the open-loop resonator. The first row, i.e., R1, is filled in an alternating fashion. The second row, i.e., R2, is completely filled in order to allow a proper flow of current between the alternately loaded cells of adjacent rows. The cells of the third row (R3) are again filled in an alternating fashion, and so on. Therefore, a geometrically and functionally novel resonator whose RCS response can be controlled through systematic loading is achieved. Based on the loading mechanism illustrated above, various resonators with shifted RCS responses can be designed. These new resonator geometries are shown in Figure 3b–d. It can be observed from Figure 3 that the RCS response shifts toward higher frequencies as the empty area becomes more and more loaded. It can be concluded that several new open-loop resonators can be formed by systematically loading the empty area of the open-loop resonator with metallic cells.

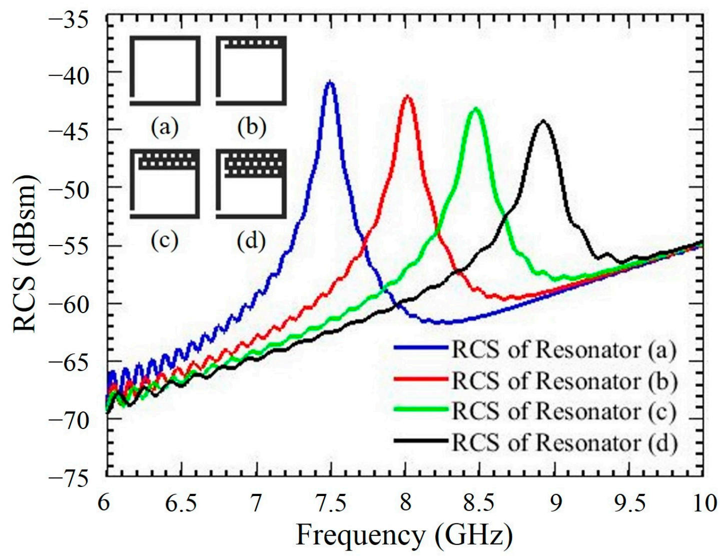


**Figure 3.** Modeling of open-loop resonators and their simulated RCS responses at various frequencies: (**a**) 7.5 GHz; (**b**) 8 GHz; (**c**) 8.4 GHz; (**d**) 8.9 GHz.

Here, for the proof of concept, a total of eight different resonators are formed to resonate at different frequencies, as shown in Figure 4. The proposed loading approach gives great flexibility to control and shape the frequency response of the tag. The overall footprint of all the newly formed open-loop resonators remains the same.

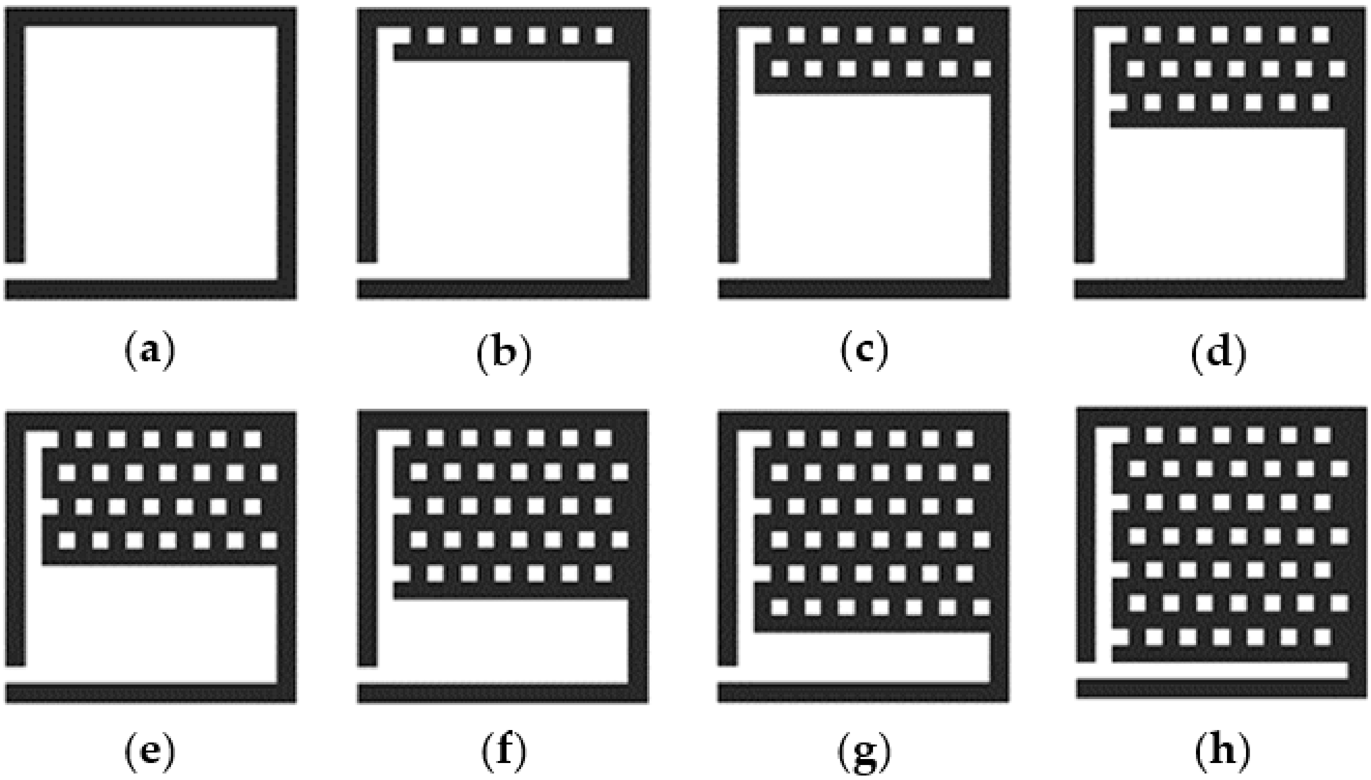


**Figure 4.** Layout of square mesh open-loop resonators: (**a**) 7.5 GHz; (**b**) 8 GHz; (**c**) 8.4 GHz; (**d**) 8.9 GHz; (**e**) 9.5 GHz; (**f**) 10.06 GHz; (**g**) 10.37 GHz; (**h**) 10.89 GHz.

To further understand the physical mechanism of the proposed tag structure, the surface current distribution is shown in Figure 5. The current distribution of the unloaded open-loop resonator excited by a linearly polarized plane wave is shown in Figure 5a. The current is entirely distributed on the loop except near the open area of the loop. The surface current density of the two partially loaded resonators is shown in Figure 5b,c, and that of a fully loaded open-loop resonator is shown in Figure 5d. From surface current analysis, three observations are made: (1) the maximum amount of current is always present on the edges of the resonators; (2) as the resonator becomes more and more loaded, the length of the current path is modified with multiple maxima and minima exciting the higher-order modes; and (3) the inner portion of the mesh grid has minimal current intensity. This phenomenon results in a frequency shift toward higher values and to attain equally distributed RCS resonances on the frequency axes, as depicted in Figure 3.

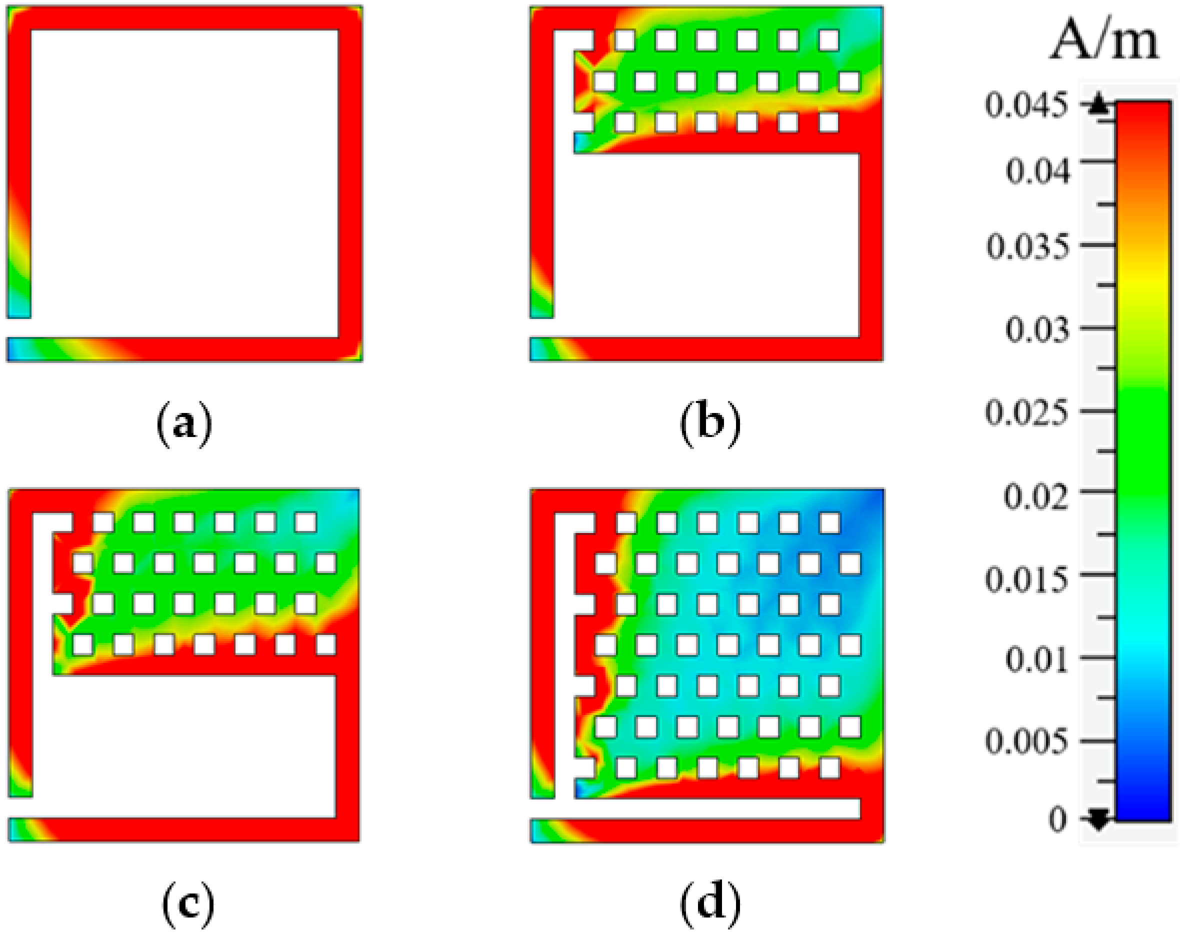


**Figure 5.** Current distribution of open-loop resonator: (**a**) 7.5 GHz; (**b**) 8.9 GHz; (**c**) 9.5 GHz; (**d**) 10.89 GHz.

## 3. Configuration Setting of Loaded Open-Loop Resonators to Form the Tags

As a proof of concept, eight systematically loaded open-loop resonators are chosen to make a tag with equally distributed RCS resonances. The eight open-loop resonators can be put into different configurations to obtain a continuous series of resonances at the frequency axis. Here, four different configurations are presented. In the first two configurations, resonators are placed on the front side of the substrate, and the backside remains empty. This is a common way of laying out the resonators. In Configuration-1, the resonators are arranged in an 8 × 1 matrix, as shown in Figure 6a. The overall size of the tag becomes 37.8 × 4.2 mm$^2$. Similarly, in Configuration-2, the resonators are arranged in a 4 × 2 matrix, as shown in Figure 6b. Here, the overall size of the tag becomes 18.6 × 9 mm$^2$. The RCS response of both configurations is shown in Figure 7. Each of the eight resonant peaks correspond to the eight resonators.

Generally, the resonators are only printed on the front side of the substrate (and the back side is left blank or metalized); however, the proposed resonators are designed in such a way that they can be printed on the backside of the substrate, hence doubling the capacity of the overall tag, providing extreme compactness and reducing the tag size by half. The printing of the resonators on the backside does not affect the working of the tag at all, as long as it is fixed on common retail items with non-conducting surfaces. In Configuration-3, four resonators are placed on the front side, and four are placed on the backside of the substrate in the form of a 2 × 2 matrix, as shown in Figure 8a. The overall size of the tag is 9 × 9 mm$^2$. In Configuration-4, four resonators are placed on the front side, and four are placed on the backside of the substrate in the form of a 4 × 1 matrix, as shown in Figure 8b. The overall size of this tag configuration is 18.6 × 4.2 mm$^2$. The effective area of both (3 and 4) configurations is the same and is half of the first two configurations. The RCS response of tag 3 and 4 is shown in Figure 9. Some resonances in the RCS of Configuration-3 are quite close to each other and are difficult to differentiate. However, the RCS response of Configuration-4 is quite distinct. Therefore, Configuration-4 is the best choice for the final tag design. The inter-resonator separation is taken as d = 1 mm for all configurations (1–4).

(**a**) Configuration-1

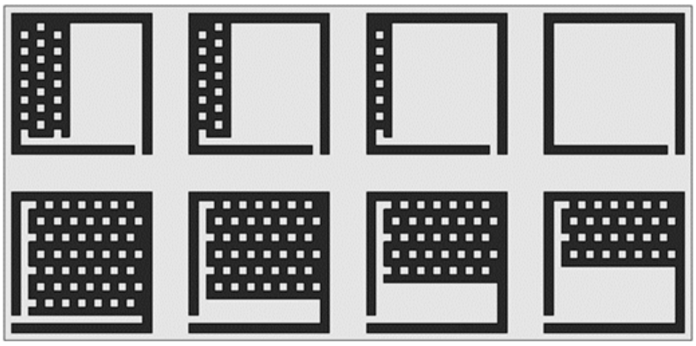

(**b**) Configuration-2

**Figure 6.** Configuration setting of loaded open-loop resonators on front side of the substrate only: (**a**) Configuration-1 (8 × 1 matrix); (**b**) Configuration-2 (4 × 2 matrix).

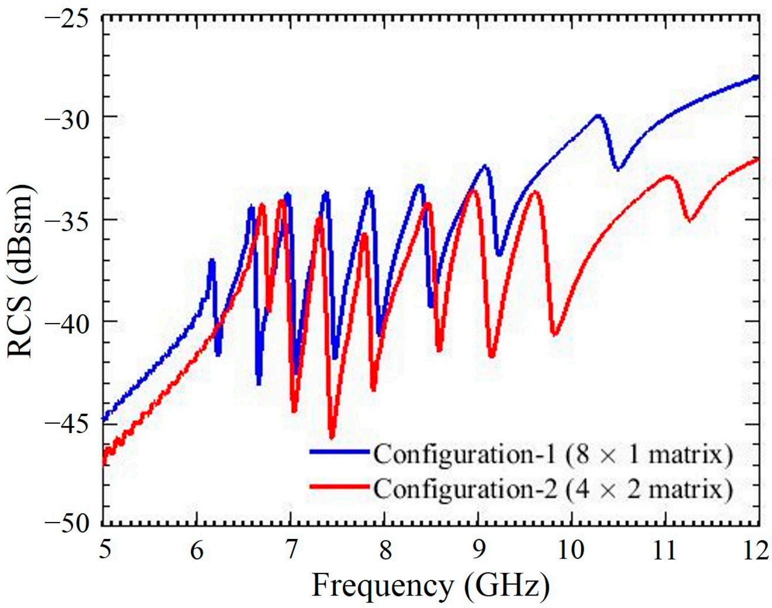


**Figure 7.** Simulated RCS response of Configuration-1 and Configuration-2.

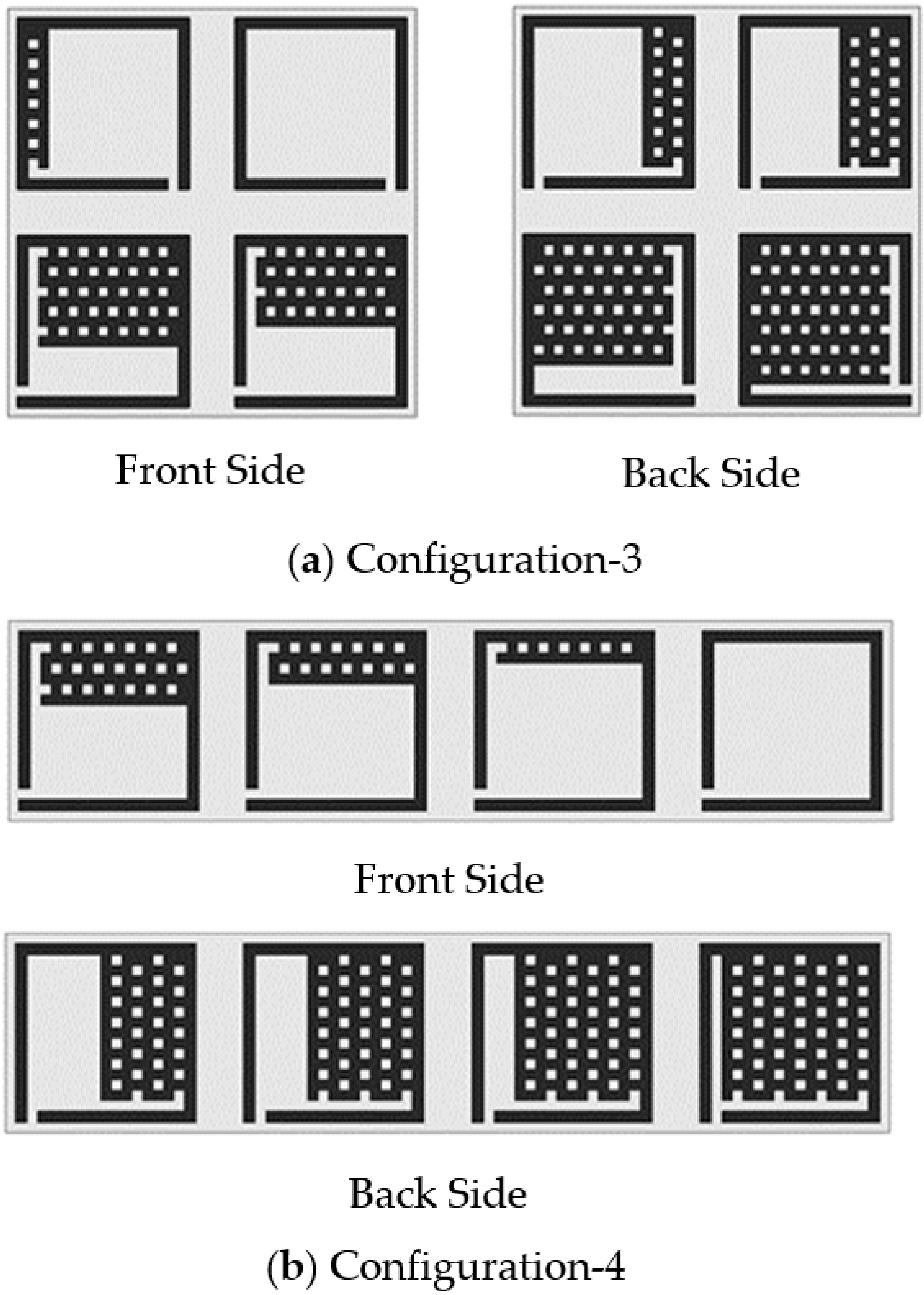


**Figure 8.** Configuration setting with loaded open-loop resonators on the front and backside of the substrate: (**a**) Configuration-3 (2 × 2 matrix); (**b**) Configuration-4 (4 × 1 matrix).

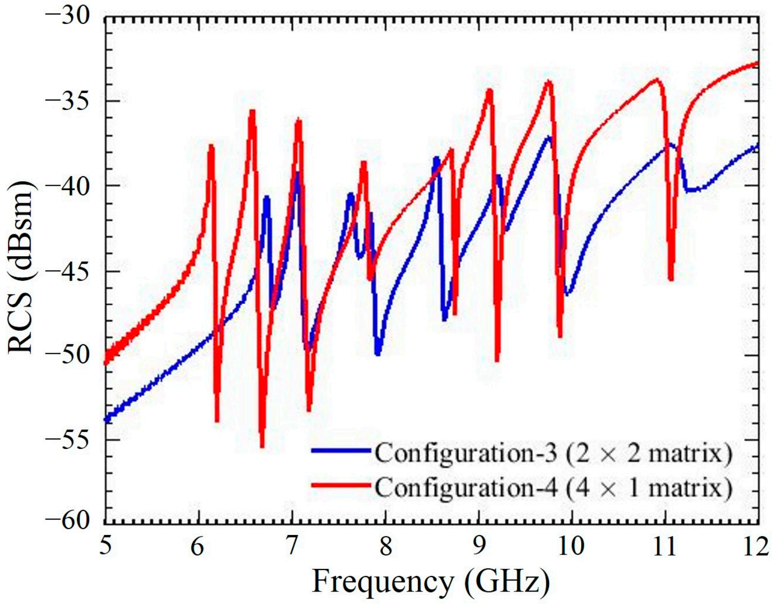


**Figure 9.** Simulated RCS response of Configuration-3 and Configuration-4.

### 3.1. *Effect of Inter-Resonator Separation*

The effect of inter-resonator separation "d" on the RCS response of the final proposed chipless tag (i.e., Configuration-4) is shown in Figure 10. It can be observed that, as the value of "d" reduces to 0.2 from the preset value of d = 1 mm, the RCS response remains stable. There is a slight increase in the RCS magnitude and a small shift toward lower frequencies. This shift is due to mutual coupling among the resonators. It is concluded that the tag can be made more compact and miniaturized by selecting smaller values of inter-resonator spacing. However, the value of d = 0.2 mm is selected by the authors for the proposed tag design. Thus, the overall size of the tag is 16.2 × 4.2 $mm^2$. The simulated RCS response is shown in Figure 11.

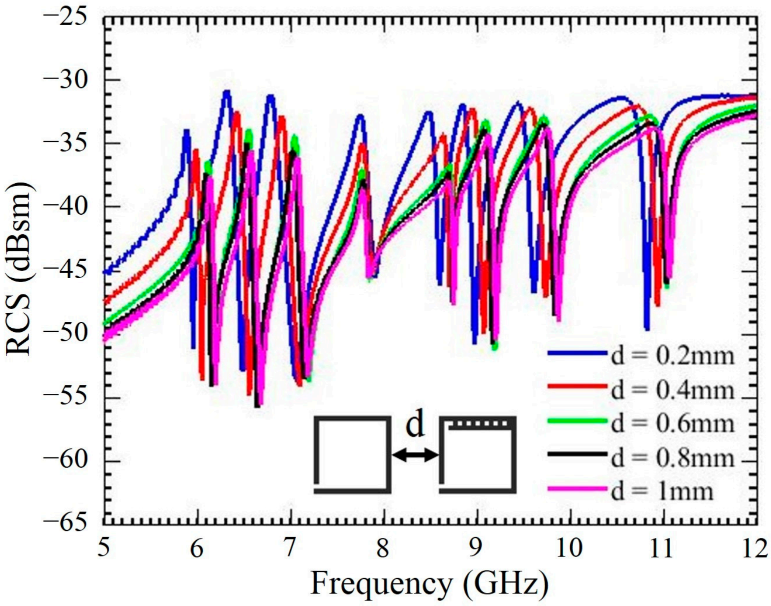


**Figure 10.** Effect of inter-resonator separation on RCS response of the tag.

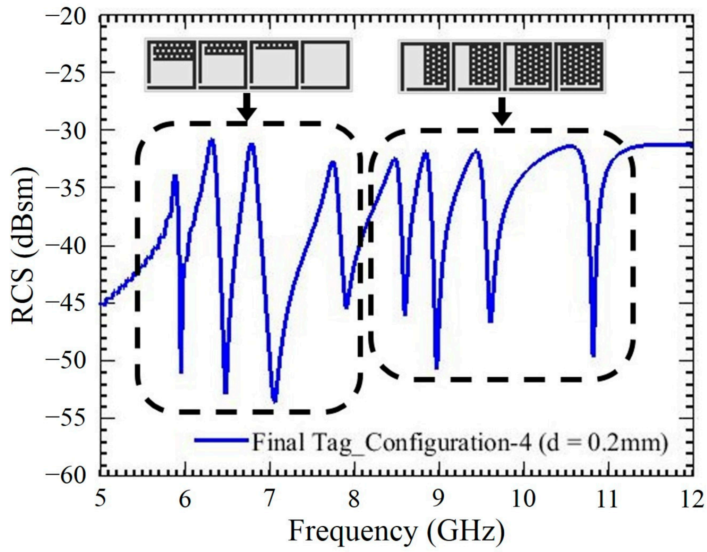


**Figure 11.** Simulated RCS response of the final proposed tag.

### 3.2. Effect of Substrate Thickness

After reaching a suitable value for the spacing between the resonators, another analysis is required to determine the effect of the substrate thickness "t" on the RCS response of the proposed tag. The RCS of the proposed tag with varying substrate thicknesses is shown in Figure 12. It can be observed that, as the value of "t" reduces to 0.2 mm, the tag RCS shifts toward the lower frequency spectrum. Moreover, the RCS magnitude level decreases, which can potentially lead to poor tag identification. Therefore, a median value of t = 0.762 mm is chosen for robust tag performance.

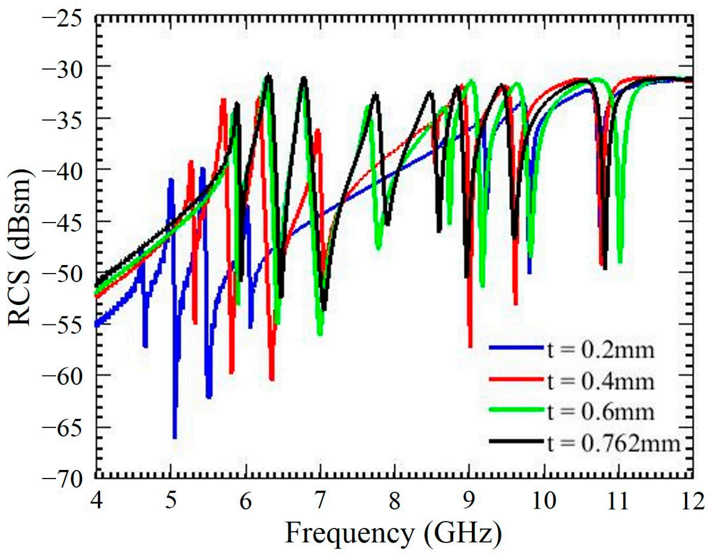


**Figure 12.** Effect of substrate thickness on RCS response of tag.

### 3.3. Illumination of the Tag from Front and Back Sides

As discussed earlier, the proposed tag is configured by placing resonators on both the front and back sides of the substrate. Therefore, knowing whether the tag reads from either side is of significant interest. The tag is illuminated from both sides by a plane wave, and the resulting RCS is plotted in Figure 13. It can be clearly seen that the RCS of the proposed tag is quite readable from both sides of the substrate. Hence, it can be concluded that the tag is side-independent and can be attached to different objects from either side.

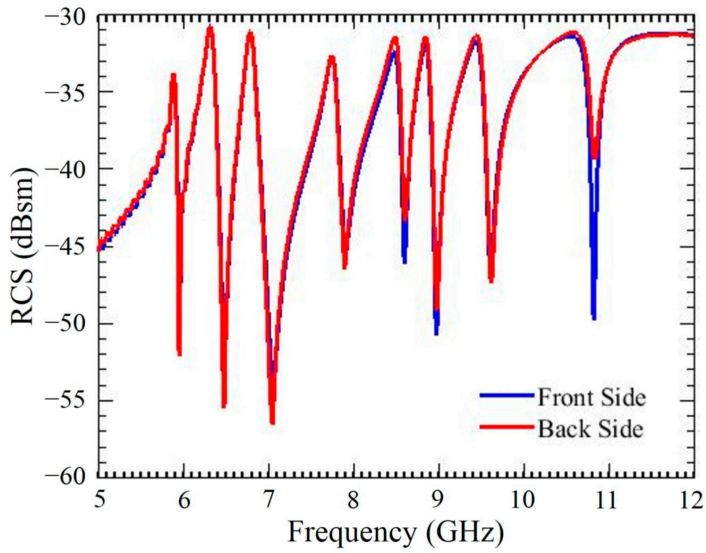


**Figure 13.** Simulated RCS response of proposed tag when illuminated from either front or back side.

### *3.4. Frequency Shift Coding (FSC) and Further Capacity Enhancement Using Intermediate Loading*

While designing frequency domain (FD)-based chipless tags, in addition to miniaturization, there are also different important specifications that must be considered to evaluate these tags, such as bit capacity, code density and spectral efficiency. These types of tags do not require any modulation scheme and solely depend on resonator geometry. All these factors can be improved either by adding extra resonators (which increases the tag size) or with different coding techniques. For a majority of conventional FD-based chipless tags, the frequency shift coding (FSC) technique is used. In the FSC technique, information is encoded within the desired band by controlling the shift in the resonance peaks of the whole tag. In the proposed design, however, the band allocated to one resonator is further sub-divided into three resonances through intermediate loading of the resonator. We define intermediate loading as the partial loading of the rows R1, R2 . . . R14. The desired frequency band (5.9–10.7 GHz) is divided into eight sub-bands (fa1–fa9), wherein each sub-band is separated by a 70 MHz guard band. The division of the tag's operating frequency band into sub-bands is outlined in Figure 14. The partial loading allows the fine adjustment of resonances in a narrower band of the frequency spectrum. These narrow band regions are obtained by designating segments within every sub-band. Each resonator can now be designed to resonate in its corresponding segment inside a sub-band through intermediate loading of the open loop. The use of segments, therefore, allows the number of combinations per resonator to be increased to any level, i.e., $2^n$. In the proposed design, each sub-band is divided into three segments with $\Delta f = 100$ MHz. Therefore, these segments represent the bit combinations 01, 10 and 11. The remaining bit combination, 00, is represented by the absence of the resonator in question. Hence, all four combinations for a given resonator, i.e., 00, 01, 10 and 11, are covered by defining three segments inside a given sub-band. Every single resonator can now be made to vary its resonance peak position within the allocated segment inside a sub-band to represent a particular bit combination.

A visual representation of the intermediate loading of resonators and their corresponding RCS responses are shown in Figure 15. The absence of a resonator (i.e., only the substrate) to represent bit combination 00 is depicted as a grey area, shown in Figure 15a. The total number of bits encoded by a resonator can be calculated using Equation (1).

$$C = 2^N \tag{1}$$

where C is the total number of combinations, and N is the number of bits per resonator. There are a total of four combinations, and therefore, 2 bits per resonator can be encoded.

Hence, the proposed tag can encode 16-bit logic code and achieves a very high code density of 23.51 bits/cm$^2$. The operating bandwidth of the proposed tag is 4.6 GHz, i.e., 5.9–10.5 GHz for encoding, and consequently, it achieves a spectral efficiency of 3.47 bits/GHz.

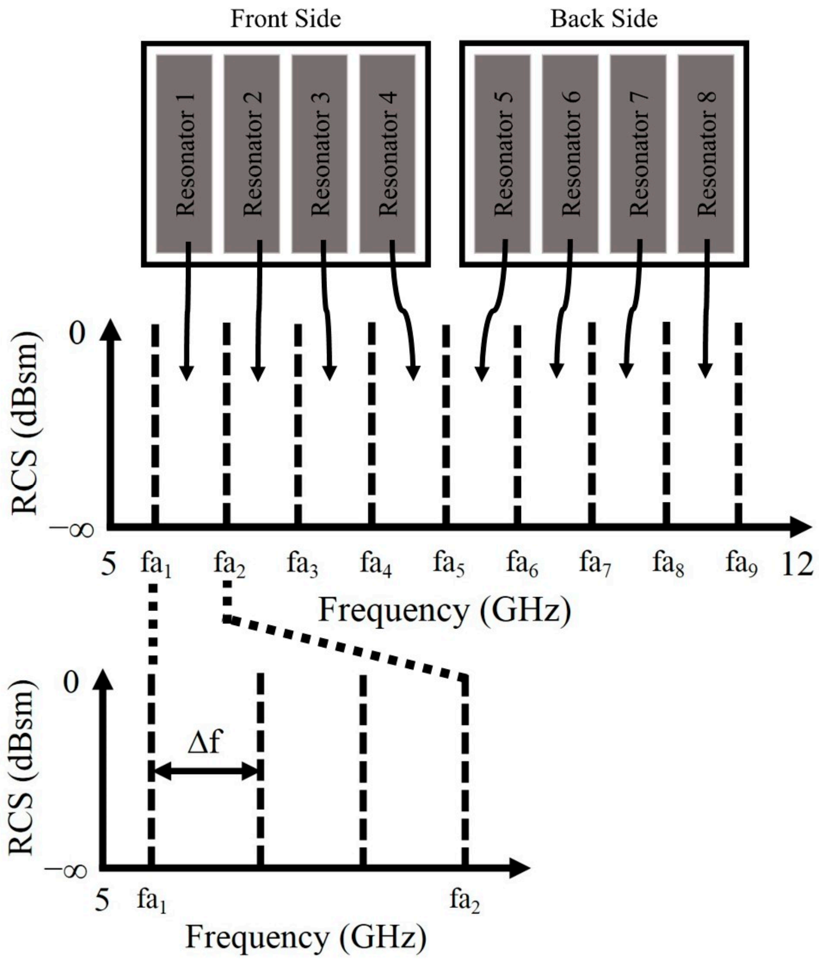


**Figure 14.** Frequency shift coding (FSC) technique to enhance capacity of the proposed chipless RFID tag.

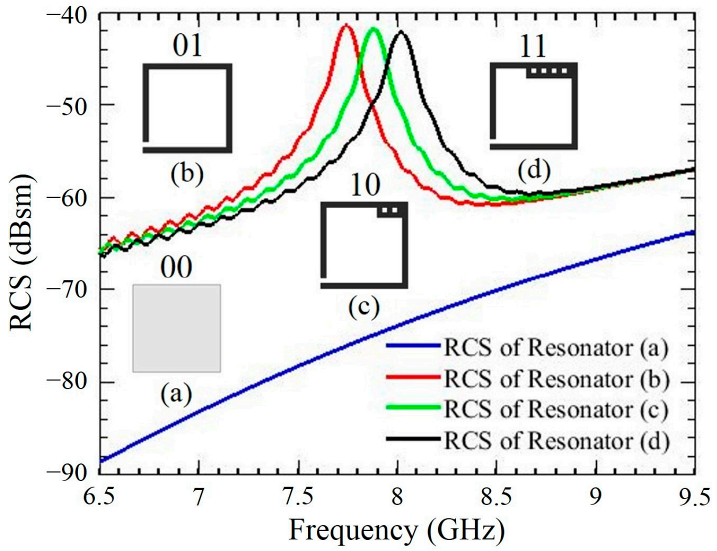


**Figure 15.** Simulated RCS response of intermediate loaded open-loop resonator.

## 4. The Experimentation

All four configurations of the proposed tag are fabricated using standard printed circuit board technology. The prototypes of the tags are shown in Figure 16. The measurements of these tags are performed in a bi-static configuration inside an anechoic chamber. The block diagram of the measurement setup is shown in Figure 17a. Two broad-band horn antennas connected to a vector network analyzer are used to record the RCS response from the tag. Both antennas have a gain of 12 dBi, and the power delivered by the VNA is around 7 dBm. A photograph of the measurement setup is shown in Figure 17b.

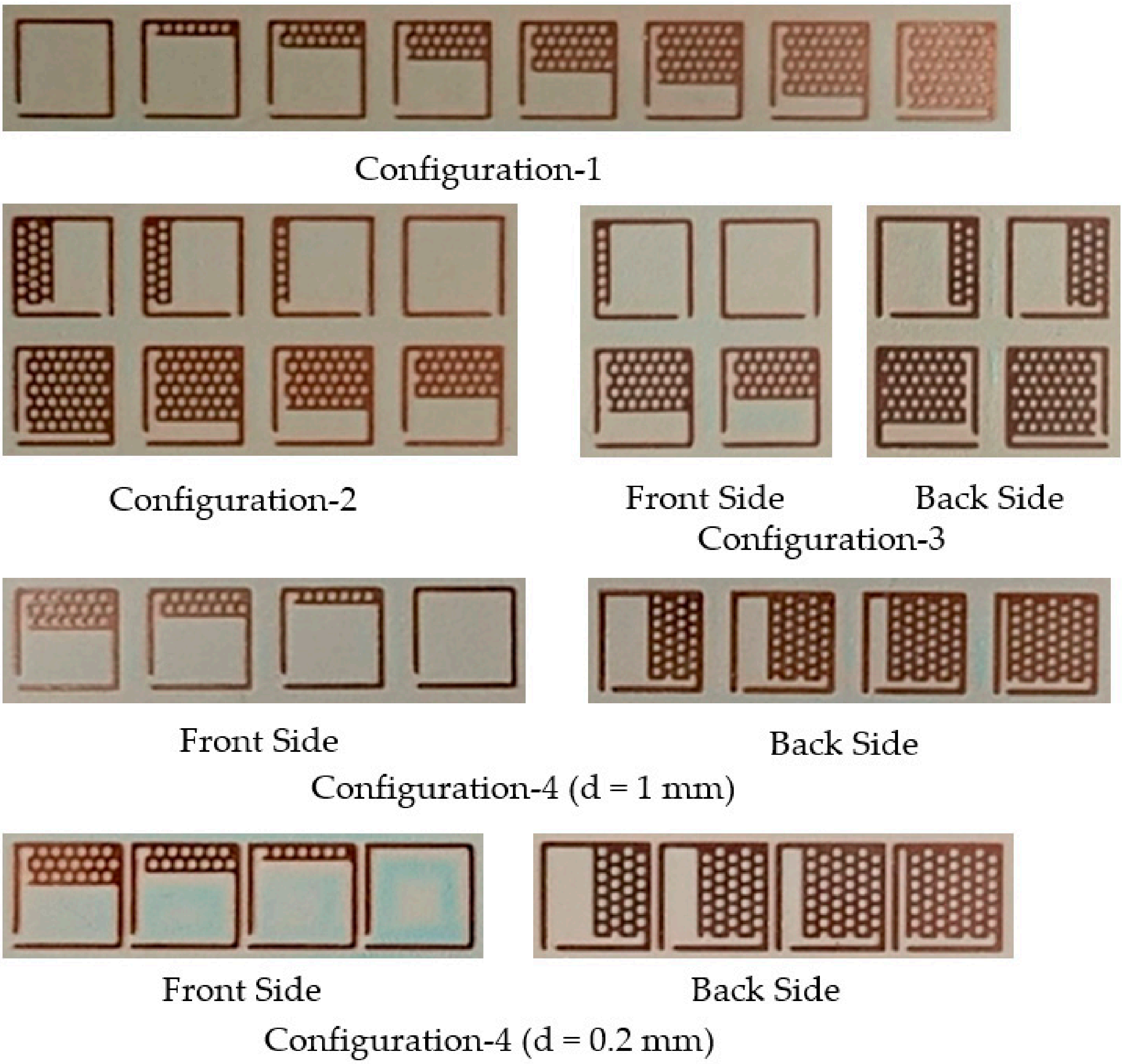


**Figure 16.** Photographs of the fabricated square mesh CRFID tags.

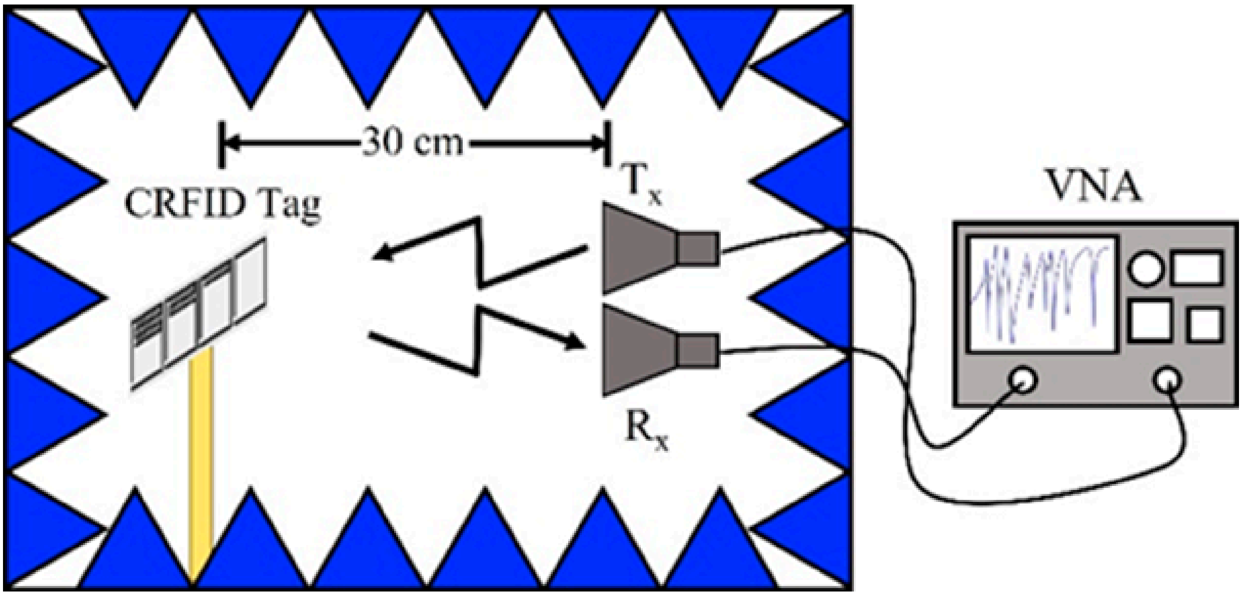


(a)

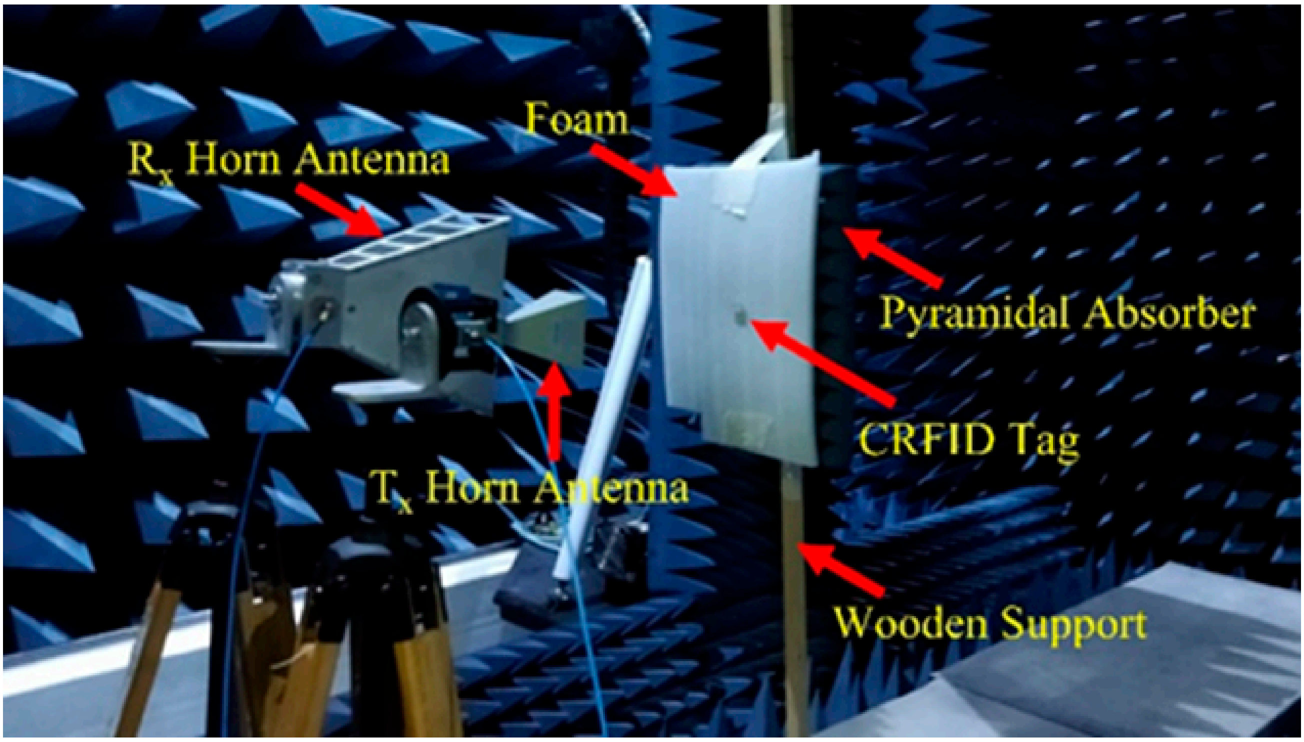


(b)

**Figure 17.** Measurement setup: (**a**) schematic of the bi-static configuration; (**b**) photograph of the RCS measurement setup inside anechoic chamber.

The tag is pasted on polystyrene foam with a negligible effect on the tag performance. Measurement without a tag is also performed to remove the effect of the foam and the environment. The measurements are calibrated by measuring the $S_{21}$ of a large metallic sheet with a known RCS. The RCS response of the tag is finally computed using the following standard formulation [17].

$$\sigma^{tag} = \left[\frac{S_{21}^{tag} - S_{21}^{isolation}}{S_{21}^{ref} - S_{21}^{isolation}}\right]^2 \cdot \sigma^{ref} \tag{2}$$

where $S_{21}^{tag}$ is the measured complex S-parameter of the proposed tag, and $S_{21}^{ref}$ is the measured complex S-parameter of the reference rectangular metallic plate. $S_{21}^{isolation}$ is the isolation measurement without the tag, $\sigma^{ref}$ is a known RCS value of the reference rectangular metallic plate, and $\sigma^{tag}$ is the computed RCS value of the proposed chipless tag. The measured RCS response of the final proposed tag (i.e., Configuration-4) for different inter-resonator separations is shown in Figure 18. The measured results are in good agreement with the simulated results. At the end, the performance of the proposed tag is compared with the published state-of-the-art chipless RFID tags in Table 1. It can be noticed that the proposed square mesh chipless tag surpasses many of those of the published work in both code density as well as spectral efficiency.

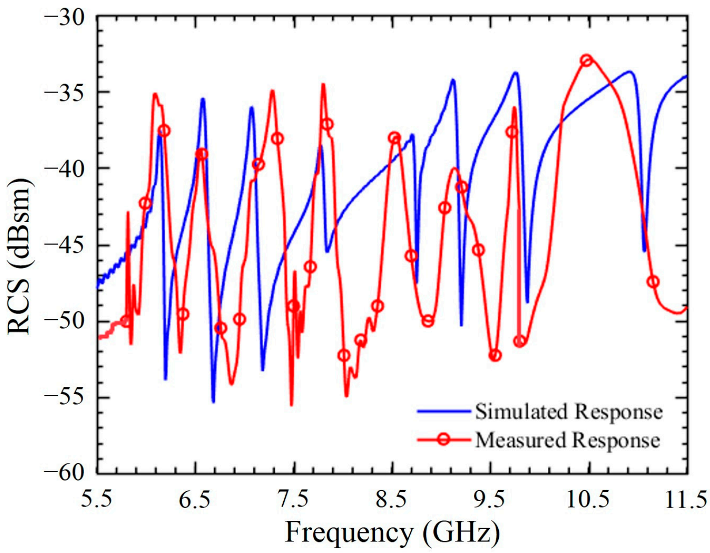


(**a**)

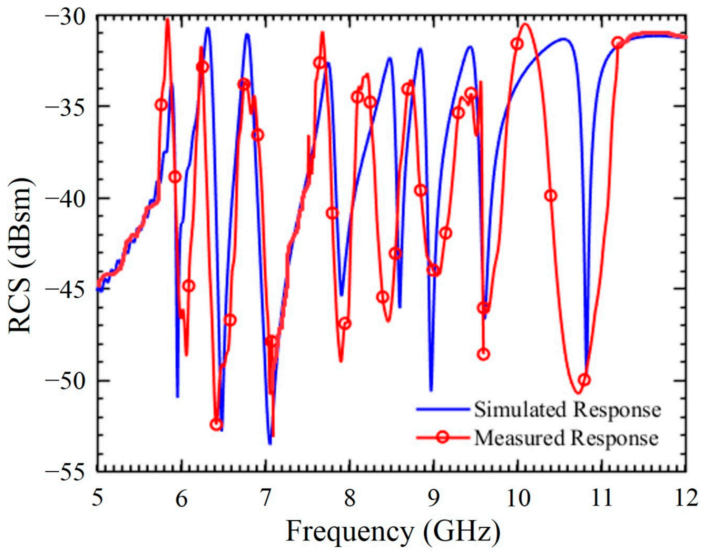


(**b**)

**Figure 18.** Measured and simulated RCS response of final proposed tag (Configuration-4): (**a**) d = 1 mm; (**b**) d = 0.2 mm.

**Table 1.** Comparison with state-of-the-art CRFID tags.

| Ref. No. | Operating Frequency (GHz) | Tag Size ($mm^2$) | Bits Per Resonator | Code Density ($bits/cm^2$) | Spectral Efficiency (bits/GHz) |
|---|---|---|---|---|---|
| [17] | 2.5–7.5 | $20 \times 40$ | 4.58 | 2.86 | 4.58 |
| [18] | 2–5 | $30 \times 40$ | 3 | 1.25 | 5 |
| [19] | 3–9 | $30 \times 30$ | 3 | 2.63 | 3.95 |
| [20] | 4.8–10 | $15 \times 10$ | 2 | 12 | 3.46 |
| [21] | 8–14 | $13.8 \times 13.8$ | 2.25 | 9.45 | 3 |
| [22] | 2.8–6 | $6.6 \times 10.8$ | 3.56 | 4.99 | 1.11 |
| [23] | 3.1–10.6 | $30 \times 25$ | 2 | 1.06 | 1.06 |
| [24] | 1.7–4.7 | $66 \times 36$ | 3 | 0.88 | 7 |
| [25] | 5–8 | $60.3 \times 11$ | 2 | 1.1 | 7 |
| [26] | 2–9 | $35 \times 35$ | 1 | 0.98 | 1.9 |
| [27] | 1.8–3.6 | $55 \times 55$ | 1 | 0.7 | 12.5 |
| [28] | 3–6 | $20 \times 20$ | 1 | 4 | 5.33 |
| [29] | 5.4–10.4 | $13.55 \times 13.55$ | 1 | 5.44 | 2 |
| [30] | 4.5–7.5 | $17 \times 14$ | 1 | 5.88 | 4.66 |
| [31] | 2–7 | $15 \times 30$ | 1 | 1.77 | 1.6 |
| Proposed Tag | 5.9–10.5 | $16.2 \times 4.2$ | 2 | 23.51 | 3.47 |

## 5. Conclusions

In this paper, a high-capacity chipless tag is presented using a novel design methodology. The tag is designed using multiple square open-loop resonators. The multi-resonance chipless tag is designed by loading an open-loop resonator with small square metallic patches. The structure that is formed resembles a square mesh with a fixed overall resonator size. The overall tag size is further miniaturized by placing the resonators on the front as well as the back sides of the substrate. The resonators are arranged in different configurations, and a highly compact tag with an overall size of $16.2 \times 4.2$ $mm^2$ is finally reached. The frequency shift coding technique is used to enhance the coding capacity of the proposed tag. A very high code density of 23.51 $bits/cm^2$ and a spectral efficiency of 3.47 bits/GHz are achieved. The proposed tag design methodology is simple and very flexible for obtaining a chipless tag with a robust performance. The proposed tags can thus be used in a variety of high-capacity tagging applications.

**Author Contributions:** M.N., U.A.H. and H.U. designed, simulated, and fabricated the prototypes. They also performed measurements and wrote the manuscript. M.I., H.R. and F.A.T. revised the whole manuscript, analyzed the results, and interpreted the data. F.A.T. also supervised the whole research project. All authors have read and agreed to the published version of the manuscript.

**Funding:** The authors acknowledge the support provided by King Abdullah City for Atomic and Renewable Energy (K.A. CARE) under the K.A. CARE-King Abdulaziz University Collaboration Program. The authors are also thankful to the Deanship of Scientific Research, King Abdulaziz University, for providing financial aid, grant number (RG-13-135-43).

**Data Availability Statement:** Not applicable.

**Conflicts of Interest:** The authors declare no conflict of interest.

## References

1. Perret, E. *Radio Frequency Identification and Sensors: From RFID to Chipless RFID*; Wiley: New York, NY, USA, 2014.
2. Noman, M.; Haider, U.A.; Hashmi, A.M.; Ullah, H.; Najam, A.I.; Tahir, F.A. A Novel Design Methodology to Realize a Single Byte Chipless RFID Tag by Loading a Square Open-Loop Resonator with Micro-Metallic Cells. *IEEE J. Microw.* **2023**, *3*, 43–51. [CrossRef]
3. Khan, M.M.; Tahir, F.A.; Farooqui, M.F.; Shamim, A.; Cheema, H.M. 3.56-bits/cm$^2$ Compact Inkjet Printed and Application Specific Chipless RFID Tag. *IEEE Antennas Wirel. Propag. Lett.* **2016**, *15*, 1109–1112. [CrossRef]

4. Noman, M.; Haider, U.A.; Ullah, H.; Tahir, F.A.; Rmili, H.; Najam, A.I. A 32-Bit Single Quadrant Angle-Controlled Chipless Tag for Radio Frequency Applications. *Sensors* **2022**, *22*, 2492. [CrossRef]
5. Haider, U.A.; Noman, M.; Ullah, H.; Tahir, F.A. A Compact L-Shaped 16 Bit Polarization Independent Chipless RFID Tag. In Proceedings of the 2020 International Conference on UK-China Emerging Technologies (UCET), Glasgow, UK, 20–21 August 2020; pp. 1–3.
6. Haider, U.A.; Noman, M.; Ullah, H.; Tahir, F.A. A Compact Chip-less RFID Tag for IoT Applications. In Proceedings of the 2020 IEEE International Symposium on Antennas and Propagation and North American Radio Science Meeting, Montréal, QC, Canada, 5–10 July 2020; pp. 1449–1450.
7. Haider, U.A.; Noman, M.; Rashid, A.; Rmili, H.; Ullah, H.; Tahir, F.A. A Semi-Octagonal 40-Bit High Capacity Chipless RFID Tag for future Product Identification. *Electronics* **2023**, *12*, 349. [CrossRef]
8. Noman, M.; Haider, U.A.; Ullah, H.; Tahir, F.A.; Khan, M.U.; Abbasi, Q.H. 12-Bit Chip-less RFID Tag with High Coding Capacity per Unit Area. In Proceedings of the 2022 IEEE International Symposium on Antennas and Propagation and USNC-URSI Radio Science Meeting (AP-S/URSI), Denver, CO, USA, 10–15 July 2022; pp. 127–128.
9. Bhattacharyya, R.; Floerkemeier, C.; Sarma, S. Towards tag antenna based sensing—An RFID displacement sensor. In Proceedings of the 2009 IEEE International Conference on RFID, Orlando, FL, USA, 27–28 April 2009; pp. 95–102.
10. Shrestha, S.; Vemagiri, J.; Agarwal, M.; Varahramyan, K. Transmission line reflection and delay-based ID generation scheme for RFID and other applications. *Int. J. Radio Freq. Identif. Technol. Appl.* **2007**, *1*, 401–416. [CrossRef]
11. Betancourt, D.; Barahona, M.; Haase, K.; Schmidt, G.; Hubler, A.; Ellinger, F. Design of printed chipless-RFID tags with QR-code appearance based on genetic algorithm. *IEEE Trans. Antennas Propag.* **2017**, *65*, 2190–2195. [CrossRef]
12. Ashraf, M.A.; Alshoudokhi, Y.A.; Behairy, H.M.; Alshareef, M.R.; Alshebeili, S.A.; Issa, K.; Fathallah, H. Design and analysis of multi resonators loaded broadband antipodal tapered slot antenna for chipless RFID applications. *IEEE Access* **2017**, *5*, 25798–25807. [CrossRef]
13. Islam, M.A.; Karmakar, N.C. Compact Printable Chipless RFID Systems. *IEEE Trans. Microw. Theory Techn.* **2015**, *63*, 3785–3793. [CrossRef]
14. Polivka, M.; Havlicek, J.; Svanda, M.; Machac, J. Improvement in robustness and recognizability of RCS response of U-shaped strip-based chipless RFID tags. *IEEE Antennas Wirel. Propag. Lett.* **2016**, *15*, 2000–2003. [CrossRef]
15. Noman, M.; Haider, U.A.; Ullah, H.; Hashmi, A.M.; Tahir, F.A. Realization of Chipless RFID Tags via Systematic Loading of Square Split Ring with Circular Slots. *IEEE J. Radio Freq. Identif.* **2022**, *6*, 671–679. [CrossRef]
16. Haider, U.A.; Noman, M.; Ullah, H.; Abutarboush, H.F.; Abbasi, Q.H.; Tahir, F.A. A Fully Passive Ten-Digit Numeric Keypad Sensor Using Chipless RFID Technology. *IEEE Sens. J.* **2023**, *23*, 2978–2987. [CrossRef]
17. Vena, A.; Perret, E.; Tedjini, S. Chipless RFID tag using hybrid coding technique. *IEEE Trans. Microw. Theory Tech.* **2011**, *59*, 3356–3364. [CrossRef]
18. Rance, O.; Siragusa, R.; Lemaître-Auger, P.; Perret, E. Toward RCS magnitude level coding for chipless RFID. *IEEE Trans. Microw. Theory Tech.* **2016**, *64*, 2315–2325. [CrossRef]
19. Ni, Y.; Huang, X.; Lv, Y.; Cheng, C. Hybrid coding chipless tag based on impedance loading. *IET Microw. Antennas Propag.* **2017**, *11*, 1325–1331. [CrossRef]
20. Issa, K.; Ashraf, M.A.; AlShareef, M.R.; Behairy, H.; Alshebeili, S.; Fathallah, H. A Novel L-Shape Ultra Wideband Chipless Radio-Frequency Identification Tag. *Int. J. Antennas Propag.* **2017**, *2017*, 2823565. [CrossRef]
21. Huang, H.; Su, L. A compact dual-polarized chipless RFID tag by using nested concentric square loops. *IEEE Antennas Wirel. Propag. Lett.* **2016**, *16*, 1036–1039. [CrossRef]
22. Wang, L.; Liu, T.; Siden, J.; Wang, G. Design of chipless RFID tag by using miniaturized open-loop resonators. *IEEE Trans. Antennas Propag.* **2018**, *66*, 618–626. [CrossRef]
23. Nijas, C.M.; Deepak, U.; Vinesh, P.V.; Sujith, R.; Mridula, S.; Vasudevan, K.; Mohanan, P. Low-cost multiple-bit encoded chipless RFID tag using stepped impedance resonator. *IEEE Trans. Antennas Propag.* **2014**, *62*, 4762–4770. [CrossRef]
24. Chen, Y.-S.; Jiang, T.-Y.; Lai, F.-P. Automatic Topology Generation of 21 Bit Chipless Radio Frequency Identification Tags Using a Noniterative Technique. *IEEE Antennas Wirel. Propag. Lett.* **2019**, *18*, 293–297. [CrossRef]
25. Abdulkawi, W.M.; Sheta, A.-F.A. Four-State Coupled Line Resonator for Chipless RFID Tags Application. *Electronics* **2019**, *8*, 581. [CrossRef]
26. Ma, Z.; Jiang, Y. High-Density 3D Printable Chipless RFID Tag with Structure of Passive Slot Rings. *Sensors* **2019**, *19*, 2535. [CrossRef] [PubMed]
27. Svanda, M.; Havlicek, J.; Machac, J.; Polivka, M. Polarisation independent chipless RFID tag based on circular arrangement of dual-spiral capacitively-loaded dipoles with robust RCS response. *IET Microw. Antennas Propag.* **2018**, *12*, 2167–2171. [CrossRef]
28. Sharma, V.; Malhotra, S.; Hashmi, M. Slot Resonator Based Novel Orientation Independent Chipless RFID Tag Configurations. *IEEE Sens. J.* **2019**, *19*, 5153–5160. [CrossRef]
29. Tariq, N.; Riaz, M.A.; Shahid, H.; Khan, M.J.; Khan, M.S.; Amin, Y.; Loo, J.; Tenhunen, H. Orientation Independent Chipless RFID Tag Using Novel Trefoil Resonators. *IEEE Access* **2019**, *7*, 122398–122407. [CrossRef]

30. Babaeian, F.; Karmakar, N.C. Compact multi-band chipless RFID resonators for identification and authentication applications. *Electron. Lett.* **2020**, *56*, 724–727. [CrossRef]
31. Tijeri-Mofrad, S.; Mohammad-Ali-Nezhad, S.; Zarif, A.H.; Khorramizadeh, M. Design of a Low-profile Chipless RFID tag Using a Grounded Wall. *IETE J. Res.* **2021**. [CrossRef]